A Meshless Local Petrov–Galerkin Method for Three-Dimensional Scalar Problems

Williams L. Nicomedes[1], Renato C. Mesquita[2], and Fernando J. S. Moreira[1]

[1]Department of Electronics Engineering, Federal University of Minas Gerais, Belo Horizonte, MG 31270-901, Brazil
[2]Department of Electrical Engineering, Federal University of Minas Gerais, Belo Horizonte, MG 31270-901, Brazil

In this paper, we apply a meshless method based on local boundary integral equations (LBIEs) to solve electromagnetic problems. The discretization process is carried out through the use of special basis functions that, unlike the Finite Element Method, are not confined to an element and do not require the support of an underlying mesh. The approach herein developed can be applied to general three-dimensional scalar boundary value problems arising in electromagnetism.

***Index Terms*—Electromagnetic field computation, local boundary integral equations (LBIEs), moving least squares.**

I. Introduction and Overview

MESHLESS (or meshfree) methods are intended to be an alternative to the widespread Finite Element Method (FEM). Although these techniques retain some basic features shared with FEM (e.g., the discretization of weak forms and global sparse matrices), a seminal difference exists between these two methods. While FEM relies on an underlying mesh in which the elements are confined, in meshfree methods both concepts are absent: there are neither meshes nor elements. These characteristics make the use of meshless methods attractive for the solution of 3-D problems, particularly for problems with boundaries varying in time (e.g., melting bodies), thus rendering re-meshing procedures unnecessary. Because meshfree techniques are relatively new, with their first applications reported in the past decade, many challenging problems still remain to be solved [1].

Meshless methods comprise a family, in which each member has a particular feature that can be explored when applied to a given problem. They have been successfully applied in mechanics, mainly in elasticity and hydrodynamics [1]. In electromagnetism, otherwise, their use is incipient [2]–[4]. In these works, a method called Element-Free Galerkin (EFG) has been employed. EFG is not truly a meshless method, because a background mesh is necessary when performing numerical integrations [1]. Another kind of meshfree method, called Meshless Local Petrov–Galerkin (MLPG) method, was devised by Atluri [5]. MLPG methods are truly meshless. There are reports on the application of MLPG to solve 2-D electrostatic problems [6] and the authors have applied MLPG4 (also known as LBIE method) to solve 2-D electromagnetic wave scattering problems [7]. The method proved to be a reliable one and the authors were even able to successfully blend it with an integral formulation [8]. In the present work, we extend the technique to 3-D electrostatic problems described by Poisson's equation.

II. Meshless Approach

Meshless methods share the same philosophy, herein described. First, nodes are spread across the domain of the problem (in this case, a region in space). The nodal distribution need not be uniform (random distributions are commonly used). A common practice employed to achieve better results is to increase the nodal density where the solution is expected to vary rapidly or near sharp edges. Second, a special function (*shape function*) is associated to each node. These functions lack analytical expressions, requiring a numerical scheme to be constructed (as addressed in Section III). Usually, a shape function associated to a node depends on the relative positions of neighboring nodes. Furthermore, shape functions are compactly supported, i.e., they are different from zero only at a small region (called *influence domain*) surrounding the node. It is this very feature that renders the stiffness matrix sparse. Third, shape functions are the elemental blocks wherewith an approximation u^h for a function u is built, i.e., given a point $\vec{r}$ in space (Fig. 1)

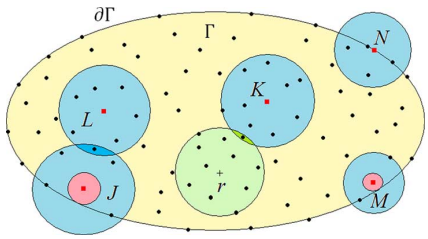

Fig. 1. Nodal influence domains and test domains.

$$u(\vec{r}) \sim u^h(\vec{r}) = \sum_{i=1}^{N} \phi_i(\vec{r})\hat{u}_i = \mathbf{\Phi}(\vec{r})\hat{\boldsymbol{u}} \tag{1}$$

where the index i runs through all nodes whose influence domains include point $\vec{r}$ (depicted inside a circle surrounding $\vec{r}$ in Fig. 1), ϕ_i is the shape function of node i (located at $\vec{r}_i$) evaluated at $\vec{r}$, and $\hat{u}_i$ is the nodal parameter to be determined. One constraint must be satisfied: the union of the influence domains from all nodes must cover the whole domain, i.e., no *holes* can be left behind, so to ensure the approximation of u everywhere inside the domain. The size of the influence domains can be adjusted, but should not be set too large, lest many nodes extend their influence domains onto $\vec{r}$, what could lead to more populated stiffness matrices. Overlapping of influence domains is freely allowed.

III. Shape Functions: The MLS Approximation

Here we have assumed all influence domains to be spheres with the same radius d_0. That is not mandatory; one is free to choose whatever form and size, albeit simpler ones are easier

Manuscript received May 31, 2010; revised July 26, 2010; accepted November 21, 2010. Date of current version April 22, 2011. Corresponding author: W. L. Nicomedes (e-mail: wlnicomedes@yahoo.com.br).

Color versions of one or more of the figures in this paper are available online at http://ieeexplore.ieee.org.

Digital Object Identifier 10.1109/TMAG.2010.2096203

0018-9464/$26.00 © 2011 IEEE

to deal with. The construction of the shape functions has been carried out through the Moving Least Squares (MLS) approximation [1]. In the MLS, u^h at a point $\vec{r}$ is expressed as

$$u^h(\vec{r}) = \sum_{j=1}^{m} p_j(\vec{r}) a_j(\vec{r}) = \boldsymbol{p}^T(\vec{r})\boldsymbol{a}(\vec{r}) \tag{2}$$

where $\boldsymbol{p}$ is a monomial basis with m terms (e.g., $[1, x, y, z]^T$) and $\boldsymbol{a}$ is a vector of coefficients which are functions of $\vec{r}$. A slightly different approximation is then built by requiring the monomial basis to be calculated at each influencing node i:

$$u^h(\vec{r}, \vec{r}_i) = \sum_{j=1}^{m} p_j(\vec{r}_i) a_j(\vec{r}) = \boldsymbol{p}^T(\vec{r}_i)\boldsymbol{a}(\vec{r}). \tag{3}$$

The next step is to define a weighted functional M, which is a sum of the squared differences between the approximations $u^h(\vec{r}, \vec{r}_i)$ and the nodal parameter $\hat{u}_i$, multiplied by a window (or weight) function w centered at $\vec{r}_i$:

$$M = \sum_{i=1}^{N} w\left(\frac{\|\vec{r} - \vec{r}_i\|}{d_i}\right) \left[\sum_{j=1}^{m} p_j(\vec{r}_i) a_j(\vec{r}) - \hat{u}_i\right]^2 \tag{4}$$

where d_i is the radius of the influence domain associated to node i (equal to d_0) and w is (for other choices, see [1])

$$w(t) = \begin{cases} 1 - 6t^2 + 8t^3 - 3t^4, & 0 \le t \le 1 \\ 0, & \text{otherwise.} \end{cases}$$

Solving for the coefficients a_j that minimize M, we impose $\partial M/\partial \boldsymbol{a} = 0$ (i.e., for each a_j). After some extensive matrix manipulations [1], one arrives at

$$\boldsymbol{a}(\vec{r}) = [\boldsymbol{A}(\vec{r})]^{-1} [\boldsymbol{B}(\vec{r})]\, \hat{\boldsymbol{u}} \tag{5}$$

where

$$\boldsymbol{u}^T = [\hat{u}_1, \hat{u}_2, \ldots, \hat{u}_N] \tag{6}$$

$$\boldsymbol{A}(\vec{r}) = \boldsymbol{P}^T \boldsymbol{W}(\vec{r}) \boldsymbol{P}, \qquad \boldsymbol{B}(\vec{r}) = \boldsymbol{P}^T \boldsymbol{W}(\vec{r}) \tag{7}$$

which are given in terms of $\boldsymbol{P}$ and $\boldsymbol{W}$

$$\boldsymbol{P} = \begin{bmatrix} p_1(\vec{r}_1) & \cdots & p_m(\vec{r}_1) \\ \vdots & \ddots & \vdots \\ p_1(\vec{r}_N) & \cdots & p_m(\vec{r}_N) \end{bmatrix} \tag{8}$$

$$\boldsymbol{W}(\vec{r}) = \begin{bmatrix} w\left(\frac{\|\vec{r}-\vec{r}_1\|}{d_1}\right) & \cdots & 0 \\ \vdots & \ddots & \vdots \\ 0 & \cdots & w\left(\frac{\|\vec{r}-\vec{r}_N\|}{d_N}\right) \end{bmatrix}. \tag{9}$$

The shape functions are obtained by equating (1) to (2)

$$\boldsymbol{\Phi}(\vec{r}) = [\phi_1(\vec{r}), \ldots, \phi_N(\vec{r})] = \boldsymbol{p}^T \boldsymbol{A}^{-1}(\vec{r}) \boldsymbol{B}(\vec{r}) \tag{10}$$

They are smooth, thanks to $w(t)$. Their first derivatives are continuous; high-order monomials in w lead to smoother higher order derivatives. The first derivatives are given by [1]

$$\boldsymbol{\Phi}_q(\vec{r}) = \boldsymbol{\gamma}_q^T(\vec{r}) \boldsymbol{B}(\vec{r}) + \boldsymbol{\gamma}^T(\vec{r}) \boldsymbol{B}_q(\vec{r}) \tag{11}$$

where the subscript q represents a partial derivative with respect to $q = x, y$, or z. The vector $\boldsymbol{\gamma}$ in (11) is found through the relation $\boldsymbol{A}(\vec{r})\boldsymbol{\gamma}(\vec{r}) = \boldsymbol{p}(\vec{r})$.

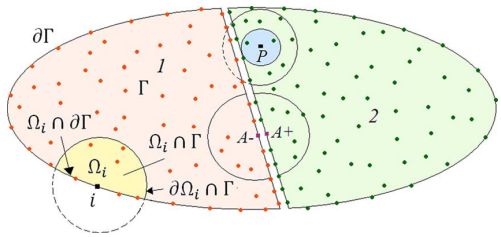

Fig. 2. Global domain Γ and a test domain Ω_i associated to a boundary node i. Sub-problems: region$(1) \cup$ region$(2) = \Gamma$.

IV. Local Boundary Integral Equation Method

A. Original Development

LBIE is a MLPG method, i.e., the expansion (shape) and the test functions belong to different spaces. The problem to be solved is stated in a region Γ of space, whose global boundary is $\partial\Gamma$ (Fig. 1). To each node i at $\vec{r}_i$, in addition to the shape function ϕ_i, a *test* function v_i is associated. This test function acts in a specific region surrounding the node, called *test domain* and represented by Ω_i (see Fig. 2). In LBIE, the test domain is required to be a *sphere* centered at the node. Other requirements that must be satisfied by v_i are as follows:

- $\nabla^2 v_i = -\delta(\vec{r} - \vec{r}_i)$ (a Dirac delta at $\vec{r}_i$);
- $v_i = 0$ at the test domain boundary $\partial\Omega_i$.

A function v_i satisfying the above requirements, and centered at a node i is therefore given by

$$v_i(\vec{r}) = \frac{1}{4\pi}\left(\frac{1}{\|\vec{r} - \vec{r}_i\|} - \frac{1}{s_i}\right) \tag{12}$$

where s_i is the radius of Ω_i. For nodes located at the interior of Γ, i.e., nodes for which there is no possibility for Ω_i to intersect $\partial\Gamma$, the test and influence domains' radii coincide (i.e., $s_i = d_i$, as illustrated for nodes K and L in Fig. 1). If the nodes are close to $\partial\Gamma$, there are two alternatives, as follows.

- The equality $s_i = d_i$ still holds, but the effective test domain will no longer be a sphere. It will be the intersection between the sphere Ω_i and the region Γ, $\Omega_i \cap \Gamma$. The boundary of the test domain becomes quite complicated: $(\partial\Omega_i \cap \Gamma) \cup (\Omega_i \cap \partial\Gamma)$.
- One makes $s_i < d_i$ and the boundary of the test domain just touches the global boundary $\partial\Gamma$ (depicted as the interior circles for nodes J and M in Fig. 1). This is suggested in [5].

In earlier works, the authors employed the first alternative, which required finding the intersections between 2-D domains ([7] and [8]), but for 3-D geometries this would be rather cumbersome. So, in the present investigation the second alternative is adopted. Regarding the nodes lying exactly at the global boundary $\partial\Gamma$, one usually takes $s_i = d_i$ and the intersection between Ω_i and Γ remains to be found (node N in Fig. 1 and domain Ω_i in Fig. 2). The approach to boundary nodes adopted here is different from that employed in [7] and [8], as explained in Section IV-B.

To get a local weak form for node i, Poisson's equation

$$\nabla \cdot [\varepsilon \nabla u(\vec{r})] = -\rho(\vec{r}) \tag{13}$$

is integrated in the test domain Ω_i. This can be carried out through two formulations. The first employs the weighted residual method, multiplying the residual of (13) by a test function v_i and integrating in Ω_i. Let the most complex case of a node lying at the global boundary to be illustrated first. (From now on, v means v_i). The volume integration is carried out in $\Omega_i \cap \Gamma$ and the surface integration is carried out in $(\partial\Omega_i \cap \Gamma) \cup (\Omega_i \cap \partial\Gamma)$. After the application of the divergence theorem

$$\iiint_{\Omega_i\cap\Gamma} \varepsilon\nabla v\cdot\nabla u dV - \oiint_{\partial\Omega_i\cap\Gamma} \varepsilon v\frac{\partial u}{\partial n}dS - \oiint_{\Omega_i\cap\partial\Gamma} \varepsilon v\frac{\partial u}{\partial n}dS = \iiint_{\Omega_i\cap\Gamma} v\rho dV \quad .(14)$$

As the test function v is zero at $\partial\Omega_i$, the first surface integral in (14) vanishes. $\partial u/\partial n$ at $\partial\Gamma$ is the boundary condition on the normal derivative. If it is known, the second surface integral goes to the right side of the equation. If a Robin condition of the type $\alpha\partial u/\partial n + \beta u = \gamma$ is employed, then $\partial u/\partial n$ may be substituted by $(\gamma - \beta u)/\alpha$. Then, for a simple problem that could admit at most a Neumann condition ($[\partial u/\partial n]_N$), the local weak form reads

$$\iiint_{\Omega_i\cap\Gamma} \varepsilon\nabla v\cdot\nabla u dV = \iiint_{\Omega_i\cap\Gamma} v\rho dV + \oiint_{\Omega_i\cap\partial\Gamma} \varepsilon v\left[\frac{\partial u}{\partial n}\right]_N dS. \quad (15)$$

For interior nodes $\Omega_i \cap \partial\Gamma = \emptyset$, the integrations are carried out in spherical test domains and the surface integral in (15) is not evaluated. In this procedure, there are no means to impose the Dirichlet conditions directly into the formulation and special methods (Lagrange multipliers, penalty factors, etc.) must be devised to enforce them.

The second formulation works only for homogeneous media. In this case, ε goes to the right side of (13) and $\nabla^2 u$ figures in the left side. Green's second identity is then applied to u and v. For the most complex case of a node lying on $\partial\Gamma$

$$-\alpha(\vec{r}_i)u(\vec{r}_i) + \iiint_{\Omega_i\cap\Gamma} v\frac{\rho}{\varepsilon}dV = \iint_{\partial\Omega_i\cap\Gamma} u\frac{\partial v}{\partial n}dS + \iint_{\Omega_i\cap\partial\Gamma} u\frac{\partial v}{\partial n}dS - \iint_{\partial\Omega_i\cap\Gamma} v\frac{\partial u}{\partial n}dS - \iint_{\Omega_i\cap\partial\Gamma} v\frac{\partial u}{\partial n}dS \quad (16)$$

where $\alpha(\vec{r}_i)$ arises out from the integration of a Dirac delta in $\nabla^2 v$, being equal to 1 for interior nodes and 0.5 for nodes lying on $\partial\Gamma$, provided the surface is smooth [5]. The third surface integral in (16) is zero because v is zero at $\partial\Omega_i$. The second surface integral carries information on u at $\partial\Gamma$ (Dirichlet condition) while the last one carries information on $\partial u/\partial n$ at $\partial\Gamma$ (Neumann or Robin). Rewriting (16) one gets

$$\alpha(\vec{r}_i)u(\vec{r}_i) + \iint_{\partial\Omega_i\cap\Gamma} u\frac{\partial v}{\partial n}dS = \iiint_{\Omega_i\cap\Gamma} v\frac{\rho}{\varepsilon}dV - \iint_{\Omega_i\cap\partial\Gamma} u\frac{\partial v}{\partial n}dS + \iint_{\Omega_i\cap\partial\Gamma} v\frac{\partial u}{\partial n}dS. \quad (17)$$

Equation (17) is a LBIE because it is stated at local domains centered at the nodes. An advantage of (17) is that Dirichlet conditions are incorporated directly into the local integral equations, thus sparing any procedure to enforce them. There is a lot of flexibility concerning the enforcement of (17) at nodes. For interior nodes, the two last integrals in (17) are not evaluated. If a node lies at a portion of $\partial\Gamma$ where Dirichlet conditions are imposed, the first term goes to the right side and the last surface integral goes to the left side. If a surface node lies where Neumann conditions are imposed, then the first surface integral goes to the left side.

V. Imposition of Boundary Conditions

In the previous section, it became clear that the intersection between Ω_i and Γ [together with local boundary $(\partial\Omega_i \cap \Gamma) \cup (\Omega_i \cap \partial\Gamma)$] must be found in order to enforce (15) or (17) for nodes at $\partial\Gamma$, but this procedure is quite cumbersome for 3-D problems. In order to avoid dealing with boundary nodes, a simple scheme, which does not require any integration, was devised [9]. It is a collocation scheme, based on the meshless approximation described by (1). Consequently, no test domains are assigned to boundary nodes. Let us suppose that a node i lies at a Dirichlet (or Neumann) boundary, whose prescribed condition is a known value $f_D(\vec{r}_i)$ (or $f_N(\vec{r}_i)$). Then

$$\sum_{j=1}^{N}\phi_j(\vec{r}_i)\hat{u}_j = f_D(\vec{r}_i) \quad \left(\text{or } \sum_{j=1}^{N}\frac{\partial\phi_j(\vec{r}_i)}{\partial n}\hat{u}_j = f_N(\vec{r}_i)\right) \quad (18)$$

where j runs through all N nodes whose influence domains include $\vec{r}_i$ (depicted inside the local domain in Fig. 2). Robin conditions are imposed likewise. This meshless collocation renders the whole procedure elegant and makes the use of LBIE method fairly simple. The integral equations (local weak forms) are enforced only at interior nodes, whose test domains are simple spheres (test domains at nodes close to the global boundary just touches $\partial\Gamma$).

VI. Handling Material Discontinuities

Care must be taken when dealing with problems where some material property (e.g., ε) is discontinuous across an interface. This is so because a shape function is smooth (i.e., the function itself and its derivatives are continuous). Shape functions inherit the order of continuity from the window function (in this work, a $C^4(\Theta)$ function, Θ being the nodal influence domain). In an electrostatic problem, at the interface between two different dielectric media the normal derivative of the electric potential is discontinuous. Consequently, the shape functions will not be able to approximate the potential accurately (usually, one observes that the numerical solution smoothens near the "knee" of the curve describing the potential, along with some oscillations). We have solved this problem as addressed in [9].

Let us assume that the problem in question is characterized by a permittivity ε which is piecewise homogeneous (refer to Fig. 2). The problem is broken up into two sub-problems, in each one of which ε is constant. Nodes from one region do not influence the other, even if their influence domains extend over there (in Fig. 2, node P lies in region 2; so, nodes from region 1 lying inside the dashed curve are disregarded).

Moreover, the test domains assigned to interior nodes from one region just touches the interface (interior circle associated to node P). The nodes lying at the interface are doubled, i.e.,

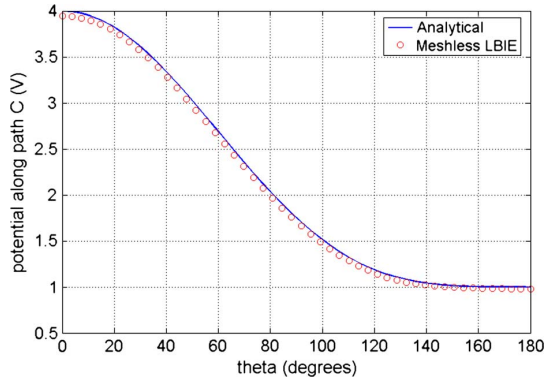

Fig. 3. First problem, solving Laplace's equation in a sphere. Analytical solution is $2(r/a)^2P_2(cos\theta) + 3(r/a)P_1(cos\theta) + 2P_0(cos\theta)$.

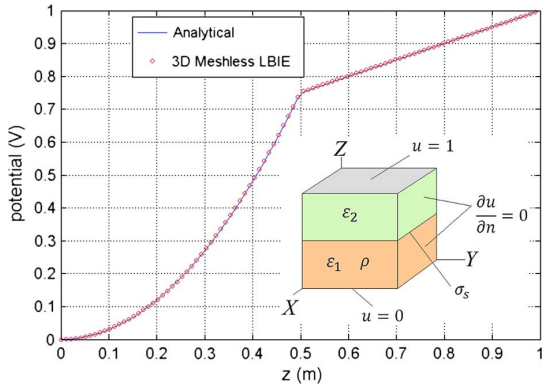

Fig. 4. Second problem, electric potential for a non-homogeneous unit cube.

each interface node is considered equivalent to two nodes, one belonging to region 1 and the other to 2 (nodes A^- and A^+). A meshless collocation method is then enforced at each dual interface node, one dealing with interface conditions on the function u and the other with conditions on the normal derivative. In electrostatics, if u is the electric potential, then u must be continuous: $u(A^-) = u(A^+)$, or

$$\sum_{i=1}^{N^-} \phi_i(A^-)\hat{u}_i = \sum_{j=1}^{N^+} \phi_j(A^+)\hat{u}_j \tag{19}$$

while $\partial u/\partial n$ is discontinuous: $\varepsilon_2 \partial u/\partial n|_{A^+} - \varepsilon_1 \partial u/\partial n|_{A^-} = \sigma_S$ (σ_S is the surface charge density at the interface), or

$$\varepsilon_2 \sum_{j=1}^{N^+} \frac{\partial \phi_j(A^+)}{\partial n}\hat{u}_j - \varepsilon_1 \sum_{i=1}^{N^-} \frac{\partial \phi_i(A^-)}{\partial n}\hat{u}_i = \sigma_S \tag{20}$$

where $i(j)$ runs through all nodes of region 1 (2) which influence $A^-(A^+)$.

VII. LBIE Discretization and Numerical Results

The potential u is represented by an expansion in MLS shape functions like (1). The local weak form (15) or (17) (without the surface integrals depending on $\partial\Gamma$) is enforced at all interior nodes. In the numerical evaluation of the integrals, care must be taken when spreading Gaussian points across the test domains, lest one of them coincides with the singularity of test function v. The boundary conditions are imposed at nodes lying on $\partial\Gamma$ through meshless collocation (18). Nodes at interfaces are treated as described by (19) and (20).

The first problem analyzed is that of a homogeneous dielectric sphere $(\varepsilon_r = 1)$ with unit radius $(a = 1)$ and no charge density inside $(\rho = 0)$, subject to the Dirichlet condition $u_D = 3cos^2\theta + 3cos\theta + 1$ V on $\partial\Gamma$. Fig. 3 shows the potential along a path C defined in spherical coordinates as $r = 0.5$ m; $0 \le \theta \le 180°$; $\varphi = 0$.

The second problem investigated takes a non-homogeneous unit cube, whose relative permittivity is 1.5 in the inferior half and 15 in the superior half (inset in Fig. 4). A charge density ρ is present in the inferior half $(\rho/\varepsilon_1 = -6\ \text{V/m}^2)$ and a surface charge density $\sigma_S = 3\ \text{C/m}^2$ at the interface.

Homogeneous Neumann conditions $(\partial u/\partial n = 0)$ were imposed at lateral faces, while Dirichlet conditions $u = 1$ V and $u = 0$ were imposed at top and bottom faces, respectively. Fig. 4 shows the potential along a path defined as $x = 0.5$ m; $y = 0.5$ m; $0 \le z \le 1$ m. For both problems, an excellent agreement between numerical and analytical solutions is observed.

VIII. Conclusion

This paper investigated the application of a meshless LBIE method to three-dimensional electrostatic problems. Similarly to FEM, this method produces sparse stiffness matrices. But a significant advantage of LBIE over FEM is that it does not require absolutely any kind of mesh, which is an important feature when solving 3-D problems. Furthermore, the treatment of boundary and interface nodes through a collocation procedure allows one to enforce the local weak forms only at the interior nodes. So, the fact of being entirely meshless together with performing the integrations only at simple spherical domains make LBIE an interesting alternative to FEM in what concerns electrostatic scalar problems.

References

[1] G. R. Liu, *Mesh Free Methods: Moving Beyond the Finite Element Method*. Boca Raton, FL: CRC, 2003.

[2] G. Parreira, E. Silva, A. Fonseca, and R. Mesquita, "The element-free galerkin method in 3-dimensional electromagnetic problems," *IEEE Trans. Magn.*, vol. 42, no. 4, pp. 711–714, Apr. 2006.

[3] O. Bottauscio, M. Chiampi, and A. Manzin, "Element-free Galerkin method in eddy-current problems with ferromagnetic media," *IEEE Trans. Magn.*, vol. 42, no. 5, pp. 1577–1584, Sep, 2006.

[4] A. Manzin and O. Bottauscio, "Element-free galerkin method for the analysis of electromagnetic-wave scattering," *IEEE Trans. Magn.*, vol. 44, no. 6, pp. 1366–1369, Jun. 2008.

[5] S. Atluri and S. Shen, "The meshless local Petrov-Galerkin method: A simple & less-costly alternative to the finite-element and boundary element methods," *CMES*, vol. 3, no. 1, pp. 11–51, 2002.

[6] A. Fonseca, S. Viana, E. Silva, and R. Mesquita, "Imposing boundary conditions in the meshless local Petrov-Galerkin method," *IET Sci. Meas. Technol.*, vol. 2, p. 387, 2008.

[7] W. Nicomedes, R. Mesquita, and F. Moreira, "A Local Boundary Integral Equation (LBIE) method in 2-D electromagnetic wave scattering, and a meshless discretization approach," in *Proc. SBMO/IEEE MTT-S Int. Microw. Optoelec. Conf.*, 2009, pp. 133–137.

[8] W. Nicomedes, R. Mesquita, and F. Moreira, "The unimoment method and a meshless Local Boundary Integral Equation (LBIE) approach in 2-D electromagnetic wave scattering," in *Proc. SBMO/IEEE MTT-S Int. Microw. Optoelec. Conf.*, 2009, pp. 514–518.

[9] Q. Li, S. Shen, Z. Han, and S. Atluri, "Application of Meshless Petrov–Galerkin (MLPG) to problems with singularities, and material Discon-Tinuities, in 3-D elasticity," *CMES*, vol. 4, no. 5, pp. 571–585, 2003.